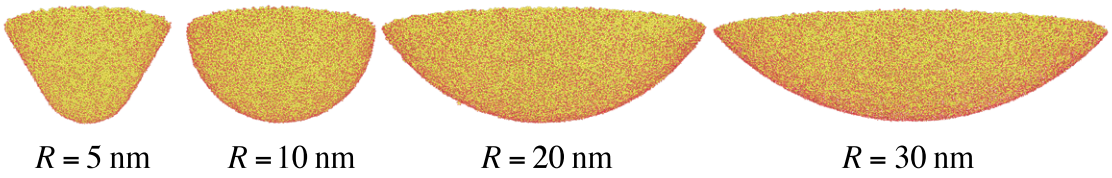

Supplementary Figure 1. Atomistic models of scanning force microscope (SFM) tips with different radii *R*. Tips are made of H-terminated amorphous carbon. Sliding simulations are performed on H-terminated diamond (111) surfaces. Temperature is held at 300K and both the tip and the sample are allowed to deform.

Methods

Molecular dynamics simulations

Simulations are carried out using the molecular dynamics (MD) technique, which is implemented in our in-house code. The essential part of MD simulations is a reliable force field (empirical potential function). We use the second generation reactive empirical bond-order potential (REBO)[1,2]. The REBO potential accurately describes cohesive energies and chemical reactions of hydrocarbon systems as well as the elastic constants of solid carbon-based materials. The range of the REBO potential extends as far as the chemical interactions and it does not include dispersive forces. The van der Waals (vdW) interactions are therefore integrated with REBO using an analytical switching function in the regime where the two potentials overlap. The parameters of the original REBO potential remain unchanged. Contributions to the vdW energy are included only for those atoms i and j that interact across the contact interface. The total vdW energy can be written as:

$$E_{\mathrm{vdW}}(r_{ij}) = -\frac{1}{2}\sum_{i}\sum_{j\neq i} C_{ij}\cdot 4\varepsilon_{ij}\left(\frac{\sigma_{ij}}{r_{ij}}\right)^{6}, \qquad \text{(S1)}$$

where r_{ij} is the interatomic distance, C_{ij} is the aforementioned switching function, and σ_{ij} and ε_{ij} are parameters equal to 3.4 Å and 1.42 meV for C-C interaction and 2.65 Å and 0.75 meV for H-H interaction, respectively. With the exception of ε_{ij}, these parameters are the same as in Ref.[3], where the adaptive intermolecular REBO (AIREBO) potential was introduced to account for vdW forces. We decreased the original value of ε_{ij} by 50% in order to correctly reproduce the experimental value of a pull-off force measured for the same systems.

In our MD studies, we use flat diamond samples and spherical tips made of diamond-like carbon (DLC). The DLC tips are prepared by cutting the desired shapes out of a bulk DLC sample. We use tips with radii of curvature R equal 5 nm, 10 nm, 20 nm, and 30 nm, and these tips are comprised of 170,467; 315,411; 787,309; and 1,261,762 atoms, respectively. All tips have the same height of 10 nm as shown in Fig. S1. The tips are first relaxed at 0K using molecular statics simulations to reduce surface energy. Subsequently H atoms are placed on the tip surface to terminate unsaturated C bonds. After H passivation, the tip is gradually heated to and equilibrated at 300K. The size of the diamond samples used in our simulations increases with the tip size. The largest sample for R = 30 nm is comprised of 4,981,800 atoms and has dimensions of 49.9 nm × 48.0 nm × 12.2 nm. In all cases we perform simulations on the (111) diamond surface, which is fully passivated with H and equilibrated at 300K prior to bringing it in contact with the tip. The bottom four layers in each sample are held rigid during simulations of normal loading and lateral sliding. Langevin thermostat is applied to a 1 nm thick layer of atoms, which is adjacent to the rigid layers. Periodic boundary conditions are applied in both lateral directions. Similar combination of rigid and thermostat layers is applied to the tip. The tip is moved by incrementally displacing atoms in the rigid layer and allowing the remaining atoms to relax dynamically.

Simulations of normal loading are performed at 300K by alternating loading and holding phases. In the loading phase, the tip is displaced toward the sample in the increments of 0.25 Å and 0.1 Å for the non-adhesive and adhesive cases, respectively. The holding phases last 10 ps and 6 ps, respectively, which is long enough for transient forces to decay and which corresponds to the average indentation speeds of 2.5 m/s and 1.7 m/s. Friction simulations are performed only for the R = 30 nm tip because such simulations are computationally very expensive. At each normal displacement, the tip is moved over the sample in the $(2\bar{1}\bar{1})$ direction, parallel to the sample surface. The sliding velocity is 20 m/s, which is comparable to the operating conditions in micromechanical systems (MEMS), but which is much larger than the typical velocity in scanning force microscopy (SFM) experiments. Bridging the gap in velocities between MD and SFM still remains one of the outstanding challenges in the field. Nevertheless, our simulation results are validated by the fact that they reproduce experimental shear strengths, contact pressures, and other parameters as discussed in the main text. In simulations of sliding we record the forces in lateral and normal directions. A stick-slip behavior is observed with the periodicity of the diamond surface of the sample. We calculate normal and friction forces by averaging them over each lattice period of the surface lattice. We report values averaged over several lattice periods and the single-period averages are used to calculate standard deviations and error bars.

Finite Element Analysis

Our tips [Fig. S1] and samples have finite sizes and it is important to determine what effect such geometry will have on contact behavior. We performed finite element analysis (FEA) on systems of two linear-elastic bodies with the same geometry, size, boundary conditions, and elastic properties as in our MD simulations. FEA calculations are done using the ABAQUS software. Loading in FEA is carried out in the same displacement increments as in non-adhesive MD simulations. The contact area vs. load relations obtained in FEA show less than 3% deviation from prediction of the Hertz model for all tip radii. The FEA results demonstrate that the effect of the finite system size, tip geometry, and boundary conditions in our MD simulations is negligible. Hence any deviations from continuum models observed in our MD simulations are due to the atomic discreteness.

Fitting to Single-Asperity Continuum Models

In the main text we discuss fitting of simulation data to continuum contact models. In the case of non-adhesive interfaces, we fit the single asperity contact area A_{asp} vs. load data with a power law function and we compare the results to the Hertz model:

$$A_{\mathrm{asp}} = \pi\left(\frac{3R}{4E^*}\right)^{2/3} L^{2/3}, \tag{S2}$$

where R is the tip radius, L is the applied load, and E^* is the effective elastic modulus, defined as:

$$E^* = \left(\frac{1-\nu_1^2}{E_1} + \frac{1-\nu_2^2}{E_2}\right)^{-1}. \tag{S3}$$

In the above equation E_1 and E_2 are the tip and the sample Young's moduli, and ν_1 and ν_2 are the tip and the sample Poisson's ratios, respectively. Using Eq. S3 we estimate E^* to be equal 303 GPa. Elastic constants that enter this equation were directly calculated in separate MD simulations and they are: for diamond E_2 (111) = 1330 GPa and ν_2 = 0.11; for amorphous carbon E_1 = 348 GPa and ν_1 = 0.33. On the other hand if we fit the simulation data to Eq. S2 for R = 30 nm tip, we obtain E^* = 134 GPa, which means that Hertz model underestimates the effective modulus by 61%.

In the case of adhesive contacts we fitted the simulation data to the Maugis-Dugdale model[4]. Because this model does not have a simple analytical form to relate contact radius a to load L, we use an approximation to this model developed by Carpick, Ogletree, and Salmeron (COS)[5]. Assuming $F_{\mathrm{f}} = \tau\left(\pi a^2\right)$, the COS fitting equation takes the form:

$$F_{\mathrm{f}} = F_{\mathrm{f0}}\left(\frac{\alpha + \sqrt{1 - L/L_{\mathrm{c}}}}{1+\alpha}\right)^{4/3}, \tag{S4}$$

where $F_{f0} = \tau\left(\pi a_0^2\right)$ is the friction force at zero load, a_0 is the contact radius at zero load, L_c is the pull-off force, and α is a transition parameter. Using procedure described in Ref.[5], α can be related to the Tabor's parameter:

$$\mu_T = \left(\frac{R\gamma^2}{\left(E^*\right)^2 z_0^3} \right)^{1/3}, \qquad \text{(S5)}$$

where γ is the work of adhesion and z_0 is the equilibrium separation of the surfaces in contact. Tabor's parameter describes a transition between two limits of contact behavior: from Johnson-Kendall-Roberts[6] (JKR) limit (for large tips and compliant materials with strong, short-range adhesion) to Derjaguin-Müller-Toporov[7] (DMT) limit (for small tips and stiff materials with weak, long range adhesion). Work of adhesion γ can be calculated from the pull-off force using expression $\gamma = L_c / \chi\pi R$, where χ ranges from 1.5 (JKR limit) to 2 (DMT limit).

We fitted the COS expression to our simulation data to calculate shear strengths and we compared the results to analogous calculations carried out on experimental data.[8] For the simulated R = 30 nm amorphous carbon tip with the measured pull-off force L_c = 24.88 nN, the COS fit yields $F_{f_0} = 3.23\,\text{nN}$ and $\alpha = 0.21$. The COS model provides also a method to calculate work of adhesion γ based on the known values of L_c, R, and α and subsequently to calculate a_0 based on the known values of γ, E^*, R, and α. We estimated E^* using Eq. S3. Finally, based on a_0 and F_{f0}, shear strength τ can be calculated using the relation $F_{f0} = \tau \cdot \left(\pi a_0^2\right)$. This procedure applied to our simulation data yields τ = 508 MPa. This value is in a very good agreement with the experimentally observed range of shear stresses of 201 MPa to 485 MPa obtained with a slightly larger tip (radius of $R = 45$ nm).

The value of $\alpha = 0.21$ obtained from fitting of the COS model to our simulation data corresponds to the Tabor's parameter μ_T = 0.19. We compared this value to the range of values of the Tabor's parameter calculated for our system directly from theory, i.e., we used Eq. S5. The upper limit of μ_T is estimated to be 0.22. Here we assumed the JKR model (χ = 1.5), which assumption allows us to calculate γ, and we set z_0 = 0.1 nm (equal to the H-H bond length). The lower limit μ_T = 0.17 was estimated by assuming the DMT model (χ = 2) and by setting z_0 = 0.17 nm (equal to the cut-off of the H-H interaction in our force field). This analysis demonstrates that the Tabor's parameter μ_T calculated from fitting continuum contact models to our simulations is in an excellent agreement with theoretical predictions made by these models.

Applicability of Macroscopic Roughness Theories to Nanoscale Contacts

In the main text we argue that continuum mechanics does not capture the correct physics of nanoscale contacts because such contacts are atomically rough. In this section we demonstrate that our results for nanoscale contacts are consistent with roughness theories, when contact area is defined in terms of atomic interactions.

A number of theories have been proposed to describe mechanics of rough contacts. One such approach, developed by Greenwood and Williamson (GW)[9], represents a surface as a sum of single asperities (protrusions), which are elastically decoupled from each other. Each asperity deforms according to the Hertzian mechanics, all asperities have the same radius of curvature, and the height distribution of asperities follows the Gaussian distribution. The GW model successfully predicts the widely observed linear relationship between the contact area and the normal load in macroscopic contacts. However, the GW model suffers from its oversimplified assumptions. For instance ignoring the elastic coupling between asperities is not physically justified. The GW model also requires defining the relevant roughness length scale *a priori* and it relies on a relatively ambiguous definition of an asperity. Other criticisms of the GW model encountered in the literature include its necessity to define a specific height distribution and a uniform size of the asperities[10-12]. In the last decade, an entirely different approach to contact of randomly rough surfaces has been proposed by Persson[11-14]. In this theory, the autocorrelation function of the surface height profile determines the pressure distribution and the area of contact. A major advantage of Persson's approach is that it treats multiple length scales of roughness simultaneously, i.e., no roughness length scale is excluded. A critical review of Persson's theory can be found in Ref.[15]

To confirm the applicability of roughness theories to nanoscale contacts, we tested predictions of these theories against the results of our MD simulations. First of all, both the GW and Persson's theories predict that contact area is proportional to the normal load. This prediction is consistent with the results of our simulations as shown in Fig. 2a in the main text. In addition, Persson' theory predicts that pressure distribution in rough contacts can be described by a double Gaussian formula,

$$P(p) = \frac{1}{\sigma\sqrt{2\pi}}\left\{\exp\left[-\frac{(p-p_0)^2}{2\sigma^2}\right] - \exp\left[-\frac{(p+p_0)^2}{2\sigma^2}\right]\right\}, \qquad \text{(S6)}$$

where p_0 and σ are the peak and width of the Gaussian distributions, respectively. Furthermore, this pressure distribution should not change with the applied load in the regime of low loads. In our simulations we define the real contact area A_{real} to be proportional to the number of atoms interacting across the interface. The nominal contact area A_{asp} between the SFM tip and a sample is defined by the edge of the contact zone. The effective radius of the nominal contact (defined as $\sqrt{A_{\text{asp}}}/\pi$) is small compared to the radius of curvature of the modeled SFM tip. As a result, the shape of the tip does not vary

significantly in the contact region and it is appropriate to use Persson's model, which was derived for flat surfaces in contact. If our results are consistent with Persson's predictions, then pressure distribution calculated for atoms interacting across the interface can be approximated by Eq. S6. To test this hypothesis, we calculated pressures for atoms in contact using a virial theorem[16]. A thermally averaged pressure distribution for the 30 nm tip and normal load L = 48 nN is shown in Fig. S2 [diamond symbols]. The solid line represents a fit to Eq. S2 and it shows that our data can be well approximated by the double Gaussian distribution predicted by Persson. The small deviations from analytical predictions observed at the tail of the distribution have been also reported in the numerically exact calculations of Campaña *et al.*[17], who used Green's function molecular dynamics to study contact mechanics of rough self-affine surfaces. These deviations are likely due to the fact that Persson's theory is not exact. Systematic corrections to this theory have been recently proposed by Müser[18].

Finally, we tested the prediction that at the early stages of normal loading pressure distribution in rough contacts is independent of the load. We fitted the double Gaussian function [Eq. S6] to normalized pressure distributions obtained in MD simulations at different loads. The center p_0 and the standard deviation σ of the distributions are plotted as a function of load in Fig. S3a and Fig. S3b, respectively. The error bars correspond to 95% confidence intervals for the fitted values. Both the center (p_0) and the width (σ) of the distributions are constant within the error bar of our calculations. As an additional test, we selected two distributions with the lowest and the highest values of p_0 and we performed a test of a statistical hypothesis that the two distributions are the same. Similar test was performed for loads with the lowest and the highest value of σ. No statistically significant difference could be found between these distributions. The invariance of pressure distribution under varying load is consistent with macroscopic roughness theories.

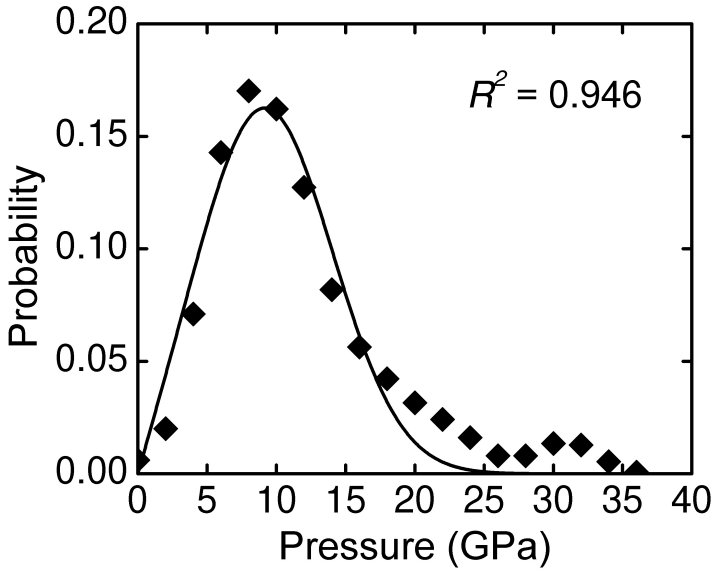

Supplementary Figure. S2. Pressure distribution of atoms in contact. Measurements are taken for a tip with the radius of curvature equal 30 nm and at a normal load of 48 nN. Diamond symbols correspond to the results of MD simulations. Solid line is a fit to Eq. S2 (The quality of the fit R^2=0.946).

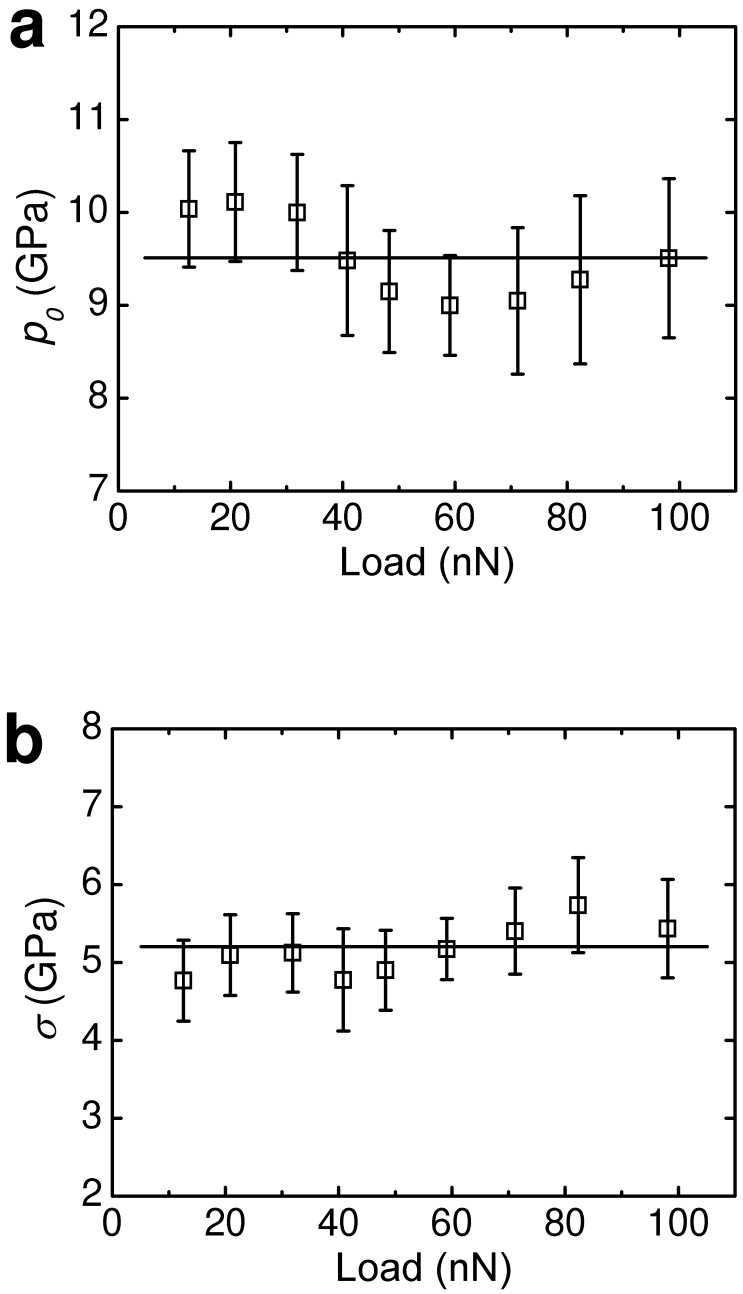

Supplementary Figure. S3. **Parameters of the double Gaussian pressure distribution (Eq. S6) as a function of the applied load. a,** Mean value p_0 and **b,** standard deviation σ. Error bars in **a** and **b** correspond to 95% confidence intervals of the best fit values calculated for pressure distributions at each load. Horizontal lines correspond to the average values of p_0 and σ.

References for Supplementary Information

1 Brenner, D.W., Empirical potential for hydrocarbons for use in simulating the chemical vapor deposition of diamond films. *Physical Review B* 42 (15), 9458 (1990).

2 Brenner, D.W., Shenderova, O.A., Harrison, J.A., Stuart, S.J., Ni, B., & Sinnott, S.B., A second-generation reactive empirical bond order (REBO) potential energy expression for hydrocarbons. *Journal of Physics-Condensed Matter* 14 (4), 783-802 (2002).

3 Stuart, S.J., Tutein, A.B., & Harrison, J.A., A reactive potential for hydrocarbons with intermolecular interactions. *J. Chem. Phys.* 112 (14), 6472-6486 (2000).

4 Maugis, D., Adhesion of spheres - the JKR-DMT transition using a Dugdale model. *J. Colloid Interface Sci.* 150, 243-269 (1992).

5 Carpick, R.W., Ogletree, D.F., & Salmeron, M., A general equation for fitting contact area and friction vs load measurements. *J. Colloid Interface Sci.* 211 (2), 395-400 (1999).

6 Johnson, K.L., Kendall, K., & Roberts, A.D., Surface energy and the contact of elastic solids. *Proc. R. Soc. Lond. A* 324 (1558), 301-313 (1971).

7 Derjaguin, B.V., Müller, V.M., & Toporov, Y.P., Effect of contact deformations on the adhesion of particles. *J. Colloid Interface Sci.* 53 (2), 314-326 (1975).

8 Gao, G.T., Cannara, R.J., Carpick, R.W., & Harrison, J.A., Atomic-scale friction on diamond: a comparison of different sliding directions on (001) and (111) surfaces using MD and AFM. *Langmuir* 23, 5394-5405 (2007).

9 Greenwood, J.A. & Williamson, J.B.P., Contact of nominally flat surfaces. *Proc. R. Soc. London Ser. A* 295, 300-319 (1966).

10 Bush, A.W., Gibson, R.D., & Keogh, G.P., Limit of elastic deformation in contact of rough surfaces. *Mech. Res. Commun.* 3 (3), 169-174 (1976).

11 Persson, B.N.J., Theory of rubber friction and contact mechanics. *J. Chem. Phys.* 115, 3840-3861 (2001).

12 Persson, B.N.J., Bucher, F., & Chiaia, B., Elastic contact between randomly rough surfaces: Comparison of theory with numerical results. *Phys. Rev. B* 65, 184106 (2002).

13 Persson, B.N.J., Elastoplastic contact between randomly rough surfaces. *Phys. Rev. Lett.* 8711 (11), art. no.-116101 (2001).

14 Persson, B.N.J., Relation between interfacial separation and load: a general theory of contact mechanics. *Phys Rev Lett* 99 (12), 125502 (2007).

15 Manners, W. & Greenwood, J.A., Some observations on Persson's diffusion theory of elastic contact. *Wear* 261 (5-6), 600-610 (2006).

16 Allen, M.P. & Tildesley, D.J. (Oxford : Clarendon Press ; New York : Oxford University Press, 1987).

17 Campaña, C., Müser, M.H., & Robbins, M.O., Elastic contact between self-affine surfaces: comparison of numerical stress and contact correlation functions with analytic predictions. *Journal of Physics-Condensed Matter* 20 (35) (2008).

18 Müser, M.H., A rigorous, field-theoretical approach to the contact mechanics of rough, elastic solids. *Phys. Rev. Lett.* 100, 055504 (2008).